

# A comparative study of the centroid and ring polymer molecular dynamics methods for approximating quantum time correlation functions from path integrals

Alejandro Pérez

*Department of Chemistry, New York University, New York, NY 10003*

Mark E. Tuckerman\*

*Department of Chemistry and Courant Institute of Mathematical Sciences, New York University, New York, NY 10003*

Martin H. Müser†

*Department of Applied Mathematics, University of Western Ontario, London, Ontario N6A 5B7, Canada*

(Dated: December 11, 2008)

The problems of ergodicity and internal consistency in the centroid and ring-polymer molecular dynamics methods are addressed in the context of a comparative study of the two methods. Enhanced sampling in ring-polymer molecular dynamics (RPMD) is achieved by first performing an equilibrium path integral calculation and then launching RPMD trajectories from selected, stochastically-independent equilibrium configurations. It is shown that this approach converges more rapidly than periodic resampling of velocities from a single long RPMD run. Dynamical quantities obtained from RPMD and centroid molecular dynamics (CMD) are compared to exact results for a variety of model systems. Fully converged results for correlations functions are presented for several one dimensional systems and *para*-hydrogen near its triple point using an improved sampling technique. Our results indicate that CMD shows very similar performance than RPMD. The quality of each method is further assessed via a new  $\chi^2$  descriptor constructed by transforming approximate real-time correlation functions from CMD and RPMD trajectories to imaginary time and comparing these to numerically exact imaginary time correlation functions. For *para*-hydrogen near its triple point, it is found that adiabatic CMD and RPMD both have similar  $\chi^2$  error.

PACS numbers:

## I. INTRODUCTION

Solving the quantum dynamics of many-body systems remains one of the most challenging problems in computational physics and chemistry due to the unfavorable computer scaling with system size and time scale of numerically exact methods. Quantum equilibrium properties, on the other hand, are routinely investigated using the path integral (PI) formalism developed by Feynman.<sup>1,2</sup> The PI interpretation fostered a new understanding of the microscopic world and provided a deep insight into various complex quantum phenomena, such as superfluidity.<sup>3</sup> Unfortunately, direct application of this formalism to real time dynamics faces a severe *sign problem* that necessitates approximation schemes.

In the last decades, several approaches have been developed to describe approximately the dynamics of quantum systems, which include: the linearized semiclassical initial value representation of Miller and Liu,<sup>4,5</sup> the quantum mode coupling theory of Reichman and Rabani,<sup>6-10</sup> the forward-backward approach of Makri and coworkers,<sup>11,12</sup> the Feynman-Kleinert linearized path integral method,<sup>13</sup> and the effective potential analytic continuation method,<sup>14</sup> among others. In the quest for simplifications to the finite-temperature quantum dynamics problem, much research effort has been directed toward devising quasi-classical approaches. Among these, centroid molecular dynamics (CMD) developed by Cao and

Voth<sup>15</sup> has attracted much attention in the last decade. The method was successfully applied to a wide variety of model systems,<sup>16</sup> and it represents a promising avenue in condensed matter physics.

In the last few years, the field of quasi-classical methods has burgeoned with recent advances in approximate methods to the quantum dynamics problem.<sup>17,18</sup> Recently, Craig and Manolopoulos<sup>19</sup> revived the primitive path integral algorithm<sup>20</sup> and applied it to approximate a variety of dynamical properties. The method has been termed ring polymer molecular dynamics (RPMD).<sup>19</sup>

A subsequent study by Braams and Manolopoulos<sup>21</sup> showed analytically that Kubo-transformed autocorrelations functions obtained from RPMD are accurate up to  $\Delta t^6$  for the position and  $\Delta t^4$  for the velocity, while the (adiabatic) centroid molecular dynamics (CMD) leads to an accuracy of only  $\Delta t^4$  and  $\Delta t^2$  for the position and velocity, respectively. Although these analytical results are clear, how they manifest in actual many body simulations remains an open question, particularly considering that there are differences between the protocols used in the theoretical analysis and those used in actual applications, as will be discussed further below.

Recently, Voth *et al.*<sup>22</sup> compared CMD and RPMD on a variety of model systems. Their study reached the conclusion that both approaches yield similar results in condensed phases although some marked differences were detected for low dimensional model systems. The

authors found that increasing the time separation between the centroid and the internal modes brings CMD results closer to the exact values, resulting in better estimates for the diffusion constant of *para*-hydrogen than RPMD.<sup>22</sup> Moreover, better estimates of the quantum kinetic energy (from the zero-time of the velocity autocorrelation function) for the same system were obtained in CMD than in RPMD. These findings partially obscure the aforementioned analysis by Braams and Manolopoulos.<sup>21</sup>

A potential weakness exists in each of the two aforementioned studies, which may lie at the origin of this controversy: The argument of Braams and Manolopoulos that CMD is less accurate at short-times than RPMD assumes that the CMD is entirely Newtonian, *i.e.*, the dynamics of internal and centroid modes are governed only by a mass tensor. However, in actual CMD simulations, thermostats are typically applied to the non-centroid modes of the ring polymer for equilibration, rendering the motion of internal modes non-Newtonian (but with increased sampling efficiency). At the same time, Voth *et al.*<sup>22</sup> did not sample RPMD in the best possible way in their comparison. It is well-known that RPMD suffers from long correlation times and naïve resampling of velocities from an equilibrium distribution (as was done in Ref.<sup>22</sup>) can easily hinder the acquisition of optimal RPMD time correlation functions.

In this comparative study, we reexamine several model systems, together with new ones, with the intention of bringing both the CMD and RPMD approaches for maximal sampling. To this end, an improved sampling technique in RPMD is introduced in order to ensure more rapid convergence of the correlation functions.

In addition to improving the sampling, we also introduce an internal consistency check to assess the quality of each path integral approach. When evaluating the quality of each path integral approach, it is desirable to have a quantitative descriptor of the method's performance, irrespective of the availability of a numerically exact solution of the dynamical problem. While for low-dimensional systems, one can easily compare approximate results to those obtained by numerically exact methods, no such comparison is possible for high-dimensional, non-harmonic systems such as liquid *para*-hydrogen.

In general, it is not recommendable to resort to a comparison with experimental data, as there is no guarantee that the force field at hand is accurate and that an agreement between computational prediction and experimental measurement is due to a fortuitous cancellation of errors in the method and/or force field. This last statement is particularly relevant when the model Hamiltonian treats a linear molecule as a spherical particle and thus neglects translation-rotation coupling. This translation-rotation coupling as well as three-body forces are likely to affect different observables in different ways so that experiments and simulations cannot be expected to match with high accuracy.<sup>23,24</sup>

A more consistent test, however, would be to use the fact that the information contained in the imaginary time correlation function is equivalent to that contained in the real-time correlation function.<sup>25</sup> Numerically exact imaginary time correlation functions are easily computed from either path-integral molecular dynamics or path integral Monte Carlo, even for complex systems, assuming an efficient path-integral sampling approach. Unfortunately, the transformation from imaginary time to real time is numerically ill-posed, which makes a direct test of the estimates for the real-time correlation functions a complicated task,<sup>26</sup> in some cases possible<sup>27–29</sup> but more commonly, inaccurate.<sup>10,30</sup> Nevertheless, the transformation from real time to imaginary time is numerically stable and can be used as a consistency check. This allows us to pose the following question:<sup>31</sup> How accurately do CMD or RPMD predict imaginary time correlation functions if these functions are not averaged directly but determined indirectly via the real-time autocorrelation function? This comparison allows us to assess the quality of a method by means of a well-defined descriptor (to be defined later) without relying on the accuracy of the model potential.

This article is organized as follows: Sec. (II A) reviews the equilibrium path integral methodology of Ref.<sup>32</sup> Sec. (II B) presents a brief review on the formalism on quantum correlation functions. This is followed by a succinct description of the approximate imaginary time path integral methods CMD (II C), RPMD (II D) and its representation in other coordinates (II E). The theory section terminates with a discussion of the ergodic problems in path integrals, our suggested sampling scheme (II F), and with the new quantitative descriptor (II G). In the accompanying Section (III), the model systems and relevant technical details are presented. The article continues in Sec. (IV) with a discussion of the main results. Finally, the conclusions are drawn in Sec. (V).

## II. BACKGROUND AND THEORY

### A. Equilibrium path-integral molecular dynamics

In this section, we briefly review the methodology of path-integral molecular dynamics. In the proceeding,  $\hat{H}$  will denote the Hamiltonian operator of the system,  $\beta = 1/k_B T$  the inverse thermal energy, and  $Z(\beta) = \text{Tr} \exp(-\beta \hat{H})$  the canonical quantum partition function. Atomic units are used throughout.

The discrete path-integral expression for the quantum canonical partition function for a single particle of mass  $m$  with Hamiltonian  $H = \hat{p}^2/2m + V(\hat{x})$  is

$$Z_P(\beta) = \left( \frac{mP}{2\pi\beta} \right)^{P/2} \int dx_1 \cdots dx_P \quad (1)$$

$$\exp \left\{ -\beta \sum_{k=1}^P \left[ \frac{1}{2} m \omega_P^2 (x_k - x_{k+1})^2 + \frac{1}{P} V(x_k) \right] \right\},$$

where  $\omega_P = \sqrt{P}/\beta$  and  $P$  is the Trotter number or number of imaginary time slices along the thermal path. The paths must satisfy the cyclic condition  $x_{P+1} = x_1$ , which arises from the trace.

Without changing any of the thermodynamic or equilibrium properties of the system, we can introduce a set of  $P$  uncoupled Gaussian integrals into Eq. (2) as follows

$$Z_P(\beta) = \mathcal{N} \int dp_1 \cdots dp_P \int dx_1 \cdots dx_P \quad (2)$$

$$\exp \left\{ -\beta \sum_{i=k}^P \left[ \frac{p_k^2}{2m'_k} + \frac{1}{2} m \omega_P^2 (x_k - x_{k+1})^2 + \frac{1}{P} V(x_k) \right] \right\},$$

where  $m'_k$  are fictitious mass parameters and  $\mathcal{N}$  is an overall normalization constant. In principle, the quantum canonical partition function could be computed via molecular dynamics (MD) using a classical Hamiltonian of the form

$$H = \sum_{k=1}^P \left[ \frac{p_k^2}{2m'_k} + \frac{1}{2} m \omega_P^2 (x_k - x_{k+1})^2 + \frac{1}{P} V(x_k) \right], \quad (3)$$

which describes the motion of a cyclic polymer chain with harmonic nearest-neighbor interactions in an attenuated external potential  $V(x)/P$ .<sup>33,34</sup> Because of the resemblance of the cyclic polymer to a necklace, the imaginary time points are colloquially referred to as “beads”, and the variables  $\mathbf{x} = x_1, \dots, x_P$  are referred to as the “primitive” path-integral variables. The parameters  $m'_k$  determine the time scale on which the imaginary time points  $x_1, \dots, x_P$  are sampled. However, as was pointed out by Hall and Berne,<sup>35</sup> the efficiency of the primitive algorithm is very poor due to the dominance of the harmonic forces from the quantum kinetic energy. Even if thermostats are coupled to each degree of freedom in the system, the wide frequency spectrum introduced by the harmonic coupling causes the MD time step to be limited by the fast modes, thereby leading to very poor sampling of the low-frequency modes.

A solution to the aforementioned problem was introduced by Tuckerman, *et al.*<sup>32</sup> and consists of three elements: 1) the variables in Eq. (3) are transformed to a set of coordinates that diagonalizes the harmonic coupling; 2) the fictitious masses  $m'_k$  are adjusted so that all modes move on the same time scale; 3) a thermostat is coupled to each mode degree of freedom in the system so as to ensure rapid sampling, equipartitioning, and a proper canonical distribution.

The equations for the transformation from “primitive” to a new set of so-called “staging” modes<sup>32</sup> can be derived from similar transformations used in path-integral Monte Carlo.<sup>36</sup> In its simplest form, the transformation to staging modes  $q_1, \dots, q_P$  (denoted collectively by  $\mathbf{Q}$ ) is

$$q_1 = x_1$$

$$q_k = x_k - \frac{(k-1)x_{k+1} + x_1}{k}, \quad k = 2, \dots, P. \quad (4)$$

When the change of variables given by Eq. (4) is introduced into Eq. (3), the partition function becomes

$$Z_P(\beta) = \mathcal{N} \int dp_1 \cdots dp_P \int dq_1 \cdots dq_P \quad (5)$$

$$\exp \left\{ -\beta \sum_{k=1}^P \left[ \frac{p_k^2}{2m'_k} + \frac{1}{2} m_k \omega_P^2 q_k^2 + \frac{1}{P} V(x_k(\{\mathbf{Q}\})) \right] \right\},$$

where  $x_k(\{\mathbf{Q}\})$  indicates the inverse transformation, and the masses  $m_k$  are defined to be

$$m_1 = 0$$

$$m_k = \frac{k}{k-1} m, \quad k = 2, \dots, P. \quad (6)$$

Note that, by this definition, the mode variable  $q_1$  drops out of the quantum kinetic energy term so that its motion is solely governed by the external potential  $V$ . In order to ensure that all modes move on the same time scale, the fictitious masses  $m'_k$  are chosen according to  $m'_1 = m$  and  $m'_k = m_k$ . Therefore, PIMD in staging modes is defined by the transformed Hamiltonian

$$H = \sum_{k=1}^P \left[ \frac{p_k^2}{2m'_k} + \frac{1}{2} m_k \omega_P^2 q_k^2 + \frac{1}{P} V(x_k(\{\mathbf{Q}\})) \right]. \quad (7)$$

In Eq. (7), the momenta  $p_k$  are treated as “conjugate” to the mode variables  $q_k$ , which means that the dynamics generated by Eqs. (7) and (3) are different because the transformation is not canonical. Finally, once the equations of motion are derived using Eq. (7), each mode variable is coupled to a separate thermostat, *e.g.*, a Nosé-Hoover chain thermostat.<sup>37</sup> In Ref.<sup>32</sup>, a more general staging type of approach was introduced by allowing staging “segments” of length  $j$  to be defined, thereby providing a natural cutoff between fast and slow modes, a generalization that was shown to possess certain advantages regarding the convergence of path integrals with large  $P$ .

The authors of Ref.<sup>32</sup> also suggested that the same scheme could be used with normal mode variables, “The staging method handles the [time-step] problem by introduction of the variable  $j$ , which naturally classifies the modes and allows only those with wavelength smaller than some cutoff to fluctuate rapidly. Such a division of time scales based on wavelength can also be constructed using normal modes.” This idea was subsequently implemented by Cao and Voth in the context of centroid molecular dynamics (see below),<sup>38</sup> by Tuckerman *et al.*, in *ab initio* path integrals methods,<sup>39</sup> by Marx *et al.* in *ab initio* centroid molecular dynamics algorithms,<sup>40</sup> and by Martyna *et al.* in the context of path integrals at constant pressure.<sup>41</sup> The transformation in this case takes the form

$$q_k = \frac{1}{\sqrt{P}} \sum_{i=1}^P U_{ki} x_i, \quad (8)$$

where the transformation  $U_{ki}$  diagonalizes the matrix arising from the quantum kinetic part:  $A_{ij} = 2\delta_{ij} - \delta_{i,j-1} - \delta_{i,j+1}$  with  $A_{i,P+1} = A_{i1}$  and  $A_{i0} = A_{iP}$ . Introducing this change of variables in Eq. (3) yields a partition function that has the same form as Eq. (6) but with

$$\begin{aligned} m_k &= m\lambda_k \\ \lambda_{2k-1} &= \lambda_{2k-2} = 2P \left[ 1 - \cos \left( \frac{2\pi(k-1)}{P} \right) \right] \end{aligned} \quad (9)$$

and  $\lambda_1 = 0$ ,  $\lambda_P = 4P$  (for even  $P$ ). As with the staging transformation, the mode  $q_1$  drops out of the quantum kinetic energy term. In fact, it is the centroid mode,  $x_0$

$$q_1 = x_0 = \frac{1}{P} \sum_{i=1}^P x_i. \quad (10)$$

In order to ensure that all modes move on the same time scale, the fictitious masses  $m'_k$  are chosen according to  $m'_k = m_k$  and  $m'_1 = m$ , which is the optimal choice for the free particle. However, depending on the system, other choices for the kinetic masses may be more efficient.<sup>42</sup> As in the staging case, each normal-mode degree of freedom is also coupled to its own thermostat.

The schemes reviewed in this section have proved highly useful in equilibrium path-integral molecular dynamics and have made the partially adiabatic centroid molecular dynamics scheme to be discussed in Sec. (II C) possible.

## B. Quantum time correlation functions

In this section, some general aspects of quantum correlation functions are succinctly reviewed.<sup>26,43</sup> The standard quantum time correlation function is defined by

$$C_{AB}(t) = \langle \hat{A}(0)\hat{B}(t) \rangle, \quad (11)$$

where  $\hat{A}$  and  $\hat{B}$  are quantum mechanical operators in the Heisenberg picture. The angular brackets denote the thermal average

$$\langle \hat{O} \rangle = \frac{1}{Z(\beta)} \text{Tr} \left[ \hat{O} \exp(-\beta\hat{H}) \right]. \quad (12)$$

In contrast to their totally symmetric classical counterparts, standard quantum correlation functions  $C_{AB}$  obey the detailed balance relation in Fourier space:  $\tilde{C}_{AB}(-\omega) = \tilde{C}_{AB}(\omega)e^{-\beta\omega}$ .

It is often more convenient, however, to work with the so-called Kubo-transformed correlation function<sup>44</sup>

$$\begin{aligned} K_{AB}(t) &= \frac{1}{\beta Z(\beta)} \times \\ &\int_0^\beta d\lambda \text{Tr} \left[ e^{-(\beta-\lambda)\hat{H}} \hat{A} e^{-\lambda\hat{H}} e^{i\hat{H}t} \hat{B} e^{-i\hat{H}t} \right], \end{aligned} \quad (13)$$

than with the original  $C_{AB}(t)$  for several reasons: First,  $K_{AB}(t)$  is purely real and invariant under time reversal. Thus, it exhibits more symmetry properties than  $C_{AB}(t)$ . Consequently, many exact expressions for  $K_{AB}(t)$  become relatively compact. Second,  $K_{AB}(t)$  is more easily compared to classical time correlation functions, which are the natural output of both CMD and RPMD calculations. Third, in the linear regime, the response of the system is directly linked to such functions via the Kubo relations.<sup>45</sup> Finally,  $K_{AB}(t)$  reduces to its classical counterpart not only in the classical limit  $\beta \rightarrow 0$  but also in harmonic systems. The Kubo-transformed and the standard correlation functions contain the same information and, in Fourier space, are related by

$$\tilde{C}_{AB}(\omega) = \left[ \frac{\beta\omega}{1 - e^{-\beta\omega}} \right] \tilde{K}_{AB}(\omega). \quad (14)$$

A quantity that is typically computed in path integral simulations is the imaginary-time quantum correlation function

$$G_{AB}(\tau) = \frac{1}{Z(\beta)} \text{Tr} \left[ e^{-\beta\hat{H}} \hat{A} e^{-\tau\hat{H}} \hat{B} e^{\tau\hat{H}} \right], \quad (15)$$

which follows from Eq. (11) after an analytic continuation to imaginary time. In particular, the imaginary time mean square displacement is easily computed from PIMD/PIMC simulations, even for complex systems

$$G(\tau) = \langle [x(\tau) - x(0)]^2 \rangle. \quad (16)$$

This important quantity is related to the real-time velocity autocorrelation function  $C_{vv}(t)$  (more precisely, its Fourier transform  $\tilde{C}_{vv}(\omega)$ ) via a two-sided Laplace transform

$$\begin{aligned} G(\tau) &= \frac{1}{\pi} \int_{-\infty}^{\infty} d\omega \exp(-\beta\omega/2) \frac{\tilde{C}_{vv}(\omega)}{\omega^2} \times \\ &\left\{ \cosh \left[ \omega \left( \frac{\beta}{2} - \tau \right) \right] - \cosh \left( \frac{\beta\omega}{2} \right) \right\}. \end{aligned} \quad (17)$$

This last equation will be used in Sec. (II G) to assess the virtues of each imaginary time method.

## C. Centroid molecular dynamics

In 1993, Cao and Voth<sup>15</sup> introduced centroid molecular dynamics (CMD) as an approximate method to compute real time quantum correlation functions. The primary object in this approach is the centroid,<sup>33</sup> defined as the average of the cyclic path  $x(\tau)$  in imaginary time  $\tau$ , see also Eq. (10)

$$x_0[x(\tau)] = \frac{1}{\beta} \int_0^\beta x(\tau) d\tau \approx \frac{1}{P} \sum_{i=1}^P x(\tau_i). \quad (18)$$

In Eq. (18) the continuous version was approximated by a discretization over  $P$  imaginary time points. The method

is rooted in the ideas developed by Feynman and Kleinert<sup>46</sup> on the effective centroid potential, which is just a potential of mean force obtained by integrating over the normal mode variables  $q_2, \dots, q_P$  defined in Eq. (8), and of Gillan<sup>47</sup>, who generalized the Feynman path concept to observables arising from time-dependent processes.

CMD relies on the assumption that the time evolution of the centroid on this potential of mean force surface can be used to garner approximate quantum dynamical properties of a system. In CMD, the centroid evolves in time according to Newtonian equations of motion<sup>16,48</sup>

$$\begin{aligned} \dot{x}_c &= \frac{p_c}{m} \\ F_0 \equiv \dot{p}_c &= -\frac{dV_0(x_c)}{dx_c}, \end{aligned} \quad (19)$$

where  $m$  is the physical mass, and  $V_0(x_c)$  is the mean field potential on the centroid at the point  $x_c$  given by

$$-\frac{1}{\beta} \ln \left\{ \left( \frac{2\pi}{m} \right)^{1/2} \oint \mathcal{D}x(\tau) \delta(x_0[x(\tau)] - x_c) e^{-S[x(\tau)]} \right\}. \quad (20)$$

In Eq. (20),  $S[x(\tau)]$  is the Euclidean time action and  $\oint \mathcal{D}x(\tau)$  denotes an functional integration over all cyclic paths whose centroid position is  $x_c$ . The mean field centroid force at  $x_c$ ,  $F_0(x_c)$ , is derived from Eq. (20) simply by spatial differentiation:

$$-\frac{\oint \mathcal{D}x(\tau) \delta(x_0[x(\tau)] - x_c) \left[ \frac{1}{\beta} \int_0^\beta \frac{dV}{dx(\tau)} d\tau \right] e^{-S[x(\tau)]}}{\oint \mathcal{D}x(\tau) \delta(x_0[x(\tau)] - x_c) e^{-S[x(\tau)]}}. \quad (21)$$

Although formally exact, Eqs. (20) and (21) are of limited use. In principle, their evaluation entails a full path integral calculation at each centroid configuration, which clearly is not feasible for complex systems.

To ameliorate the computational burden of the Eqs. (20) and (21) in practical MD calculations, the adiabatic approximation is often invoked.<sup>49</sup> The masses of the internal modes are made significantly lighter than centroid mass so as to facilitate an efficient exploration of phase space as required by Eq. (21). To achieve this limit, an adiabaticity parameter  $\gamma^2$  ( $0 < \gamma^2 < 1$ ) is introduced to scale down the fictitious kinetic masses of the internal modes  $m'_k = \gamma^2 m \lambda_k$  and therefore to accelerate their dynamics.<sup>22</sup> Ref.<sup>40</sup> contains one particular proof of the adiabatic method. In practice, however, a partial separation is normally accomplished and the scheme has been termed partially adiabatic centroid molecular dynamics (PACMD).<sup>22</sup> In this work, however, we obviate this distinction and simply refer to PACMD as CMD for brevity.

Eq. (21) also demands a canonical sampling over the internal modes. As discussed in Sec. (II A), thermostats are typically attached to the internal (non-centroid) modes to achieve a rapid equilibration whereas the centroid is

normally unthermostated so as not disrupt the dynamical properties of the system. More technical details on the method are discussed in Refs.<sup>40,41,49</sup>

Finally, in the CMD formalism, the expectation value of any observable  $O$  is expressed as an ensemble average over the centroid variables

$$\langle O \rangle \approx \frac{1}{Z} \iint \frac{dx_c dp_c}{2\pi} O(p_c, x_c) e^{-\beta \left[ \frac{p_c^2}{2m} + V_0(x_c) \right]}. \quad (22)$$

In particular, the Kubo-transformed quantum time correlation function between two operators  $\hat{A}$  and  $\hat{B}$  is approximated by

$$\langle A(0) B(t) \rangle \approx \frac{1}{(2\pi)^P Z} \int \frac{dx_c dp_c}{2\pi} A(x_c(0), p_c(0)) \times B(x_c(t), p_c(t)) e^{-\beta \left[ \frac{p_c^2}{2m} + V_0(x_c) \right]}, \quad (23)$$

where the operator  $\hat{B}$  is evaluated using the time-evolved centroid variables according to Eq. (20), starting from  $\{x_c(0), p_c(0)\}$  as initial conditions.

#### D. Ring polymer molecular dynamics

RPMD starts with the primitive path-integral algorithm of Eq. (3). In their recent article,<sup>19</sup> Craig and Manolopoulos extended the significance of the primitive method to the real time domain based on its correct limits in the harmonic and classical cases. The method was later applied to study the self-diffusion of quantum fluids,<sup>50,51</sup> the inelastic neutron scattering of *para*-hydrogen<sup>52</sup>, and to formulate a quantum version of the transition state theory.<sup>53</sup>

The principal differences that distinguish RPMD from CMD are threefold. First, the RPMD kinetic masses are chosen such that each imaginary time slice or bead has the physical mass  $m$ . Second, RPMD uses the full chain to estimate expectation values:

$$O_P(t) = \frac{1}{P} \sum_{i=1}^P \hat{O}[x_i(t)]. \quad (24)$$

For example, in RPMD the Kubo-transformed velocity autocorrelation function is approximated by

$$K_{vv}(t) \approx \frac{1}{(2\pi)^P Z_P} \int d\mathbf{x} \int d\mathbf{p} v_P(0) v_P(t) e^{-\beta_P H_P(\mathbf{x}, \mathbf{p})}, \quad (25)$$

where  $\beta_P = \beta/P$  (RPMD simulations are typically carried out at  $P$  times the actual temperature) and

$$H_P(\mathbf{x}, \mathbf{p}) = \sum_{j=1}^P \frac{p_j^2}{2m} + \frac{m}{2\beta_P^2} \sum_{j=1}^P (x_j - x_{j-1})^2 + \sum_{j=1}^P V(x_j). \quad (26)$$

Note that the harmonic bead-coupling and potential energy terms are taken to be  $P$  times larger than their counterparts in Eq. (3). We adopt this convention for consistency with Ref.<sup>19</sup>, however note that this amounts to nothing more than a rescaling of the temperature from  $T$  to  $PT$ . Obviously, for operators linear in position and/or momentum, the CMD and RPMD representations of observables is the same, however, they usually differ for functions that are non-linear in those coordinates.

The third difference is that RPMD is purely Newtonian. The equations of motion are easily derived from the previous Hamiltonian, Eq. (26)

$$\begin{aligned}\dot{p}_j &= -\frac{m}{\beta_P^2} [2x_j - x_{j-1} - x_{j+1}] - \frac{\partial V}{\partial x_j} \\ \dot{x}_j &= \frac{p_j}{m},\end{aligned}\quad (27)$$

where  $j = 1, \dots, P$ . No thermostats are used on any of the beads because all beads are treated as dynamical variables in RPMD.

### E. Ring polymer molecular dynamics in other coordinates

The RPMD scheme presented in the last subsection was defined using Cartesian (or primitive) coordinates, see Eq. (26)

$$H(\mathbf{x}, \mathbf{p}) = \frac{\mathbf{p}^t \mathbf{p}}{2m} + \frac{m}{2} w_P^2 \mathbf{x}^t \kappa \mathbf{x} + V(\mathbf{x}), \quad (28)$$

where  $w_P^2 = (P/\beta)^2$  and  $\kappa$  is the stiffness matrix. However, it is possible to carry out the same dynamics using other coordinates provided that the transformation is canonical, *i.e.*, the Poisson brackets are preserved. Unlike in Sec. (II A), here not only are the positions changed but the momenta are transformed accordingly in order to generate the same dynamics as in Eq. (26). In this subsection, we discuss how the RPMD Hamiltonian transforms using normal mode (NM) and staging coordinates, which are the most commonly used variables in path integral calculations.

The NM transformation was introduced in Eq. (8), where  $U$  is a unitary matrix with elements  $U_{1j} = 1/\sqrt{P}$  and  $U_{Pj} = (-1)^j/\sqrt{P}$  for  $j = 1, \dots, P$ ; and  $U_{2i,j} = \sqrt{2/P} \cos(2\pi ij/P)$  and  $U_{2i+1,j} = \sqrt{2/P} \sin(2\pi ij/P)$  for  $1 \leq i < P/2$ . The RPMD Hamiltonian in NM coordinates reads

$$H(\mathbf{Q}, \mathbf{P}) = \frac{1}{2} \mathbf{\Pi}^t \mathcal{M}^{-1} \mathbf{\Pi} + \frac{m}{2} w_P^2 \mathbf{Q}^t \mathcal{K} \mathbf{Q} + V(\mathbf{x}(\mathbf{Q})), \quad (29)$$

where  $\mathbf{\Pi} = \pi_1, \dots, \pi_P$  are the transformed momenta and  $\mathcal{M} = mP\mathcal{I}$  is the new mass tensor, with  $\mathcal{I}$  the identity matrix. The stiffness matrix in these coordinates  $\mathcal{K} =$

$PU\kappa U^t$  ( $t$  denotes matrix transpose) becomes diagonal and its elements  $\mathcal{K}_j$  are given by Eq. (9). The equations of motion (EOM) generated by this new Hamiltonian are

$$\begin{aligned}\dot{\pi}_i &= -mw_P^2 \mathcal{K}_i q_i - \sqrt{P} \sum_{j=1}^P U_{ij} \nabla_{x_j} V(\mathbf{x}(\mathbf{Q})) \\ \dot{q}_i &= \sum_{j=1}^P \mathcal{M}_{ij}^{-1} \pi_j = \frac{\pi_i}{mP}.\end{aligned}\quad (30)$$

The advantage of using NM coordinates is that the centroid mode separates out naturally and multiple time scale integration methods<sup>54</sup> can be easily incorporated in the integration scheme of the harmonic kinetic part.<sup>50</sup> Finally, the equipartition theorem, which in Cartesian velocities is  $m\langle v^2 \rangle = TP$ , now becomes  $m\langle \mathbf{V}^t \mathbf{V} \rangle = T$  where  $\mathbf{V} = \dot{\mathbf{Q}} = U\dot{\mathbf{x}}/\sqrt{P}$  denotes the NM velocities.

As stated in Sec. (II A), one of us<sup>32</sup> introduced the staging transformation in PIMD for efficient sampling of equilibrium quantities of quantum system. The staging coordinates are defined by  $\mathbf{Q} = \mathcal{T}\mathbf{x}$ , with the associated canonical momenta  $\mathbf{\Pi} = \mathcal{T}^{-1}\mathbf{p}$ . The transformation matrix  $\mathcal{T}$  is non-orthogonal, but nonetheless, it accomplishes a total diagonalization of the stiffness matrix  $\kappa$ . The resulting diagonal elements are, however, not the eigenvalues of original matrix  $\kappa$ .

The RPMD Hamiltonian in staging coordinates resembles the one in Eq. (29), except for a new mass tensor  $\mathcal{M} = m\mathcal{T}^{-1t}\mathcal{T}^{-1}$ , which is symmetric but not diagonal. The new stiffness matrix  $\mathcal{K} = \mathcal{T}^{-1t}\kappa\mathcal{T}^{-1}$  becomes diagonal in this representation with elements  $\mathcal{K}_i = i/(i-1)$  for  $i = 2, \dots, P$  and  $\mathcal{K}_1 = 0$ . The EOM formulated in staging variables are given by

$$\begin{aligned}\dot{\pi}_i &= -mw_P^2 \mathcal{K}_i q_i - \sum_{j=1}^P \mathcal{T}_{ij}^{-1t} \nabla_{x_j} V(\mathbf{x}(\mathbf{Q})) \\ \dot{q}_i &= \sum_{j=1}^P \mathcal{M}_{ij}^{-1} \pi_j,\end{aligned}\quad (31)$$

where  $\mathcal{M}^{-1} = m^{-1}\mathcal{T}\mathcal{T}^t$  is the inverse mass tensor in staging variables. Finally, the equipartition theorem in staging velocities reads  $\langle \mathbf{V}^t \mathcal{M} \mathbf{V} \rangle = PT$ .

Fig. 1 displays the Kubo-transformed position autocorrelation function for the quartic potential  $0.25x^4$  computed from RPMD using primitive, NM, and staging coordinates. As the transformations were carried out canonically, the dynamical quantities should be reproduced exactly in the same manner as is shown in the figure. The minor discrepancies between curves are due to the sampling over different initial conditions.

### F. Ergodicity problem in path-integral simulations

Ergodicity is a problem that plagues both CMD and RPMD simulations.<sup>32</sup> While we do not wish to affect the

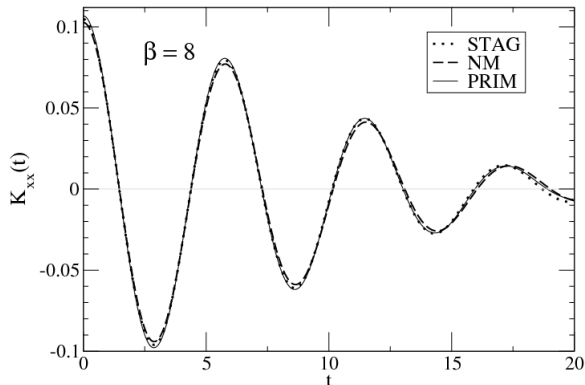


FIG. 1: Kubo-transformed position autocorrelation function for quartic potential  $V(x) = 0.25x^4$ ,  $\beta = 8$ , and  $P = 32$  computed from RPMD in various coordinates: Primitive (solid), Normal Modes (dashes), and Staging (dots). The minor discrepancies between curves are due to the sampling over different initial conditions.

dynamics of the system, it is imperative to have adequate statistics. One possible way to satisfy these conflicting requirements is to employ a combined approach whereby a mild dissipative particle dynamics (DPD) thermostat<sup>55,56</sup> is used on the centroid and Langevin or Nosé-Hoover chain<sup>37</sup> thermostats are applied to the internal modes to achieve a rapid equilibration. This approach, however, was not pursued in this work. Rather, we focus our attention on the acquisition of averages and correlation functions.

In previous studies, averages were accumulated in a sequential manner starting from a limited portion of coordinate space and proceeding thereafter with only a resampling of the velocities. This protocol, although straightforward, may be problematic due to the slow convergence of path integrals in general, with particular severity near phase transitions.

In this study, an improved sampling method is proposed to ensure a proper sampling of configuration space. Fig. 2 depicts the scheme. First, a long equilibrium PIMD simulation is performed, as described in Sec. (II A), with the sole purpose of generating uncorrelated initial configurations. Equilibrium PIMD algorithms use internal staging or normal-mode variables for optimal sampling. Based on the previous discussion, periodically stored configurations in these coordinates can then be used in the CMD or RPMD simulations, or, for RPMD, they can be transformed back to primitive variables. The initial velocities can be either drawn from the Maxwell-Boltzmann distribution or taken from the equilibrium PIMD run provided that a brief adjustment of the initial velocities is allowed (short equilibration or “Verlet warm up” in the figure) due to the different mass tensor in the dynamical algorithms. Periodic resampling of velocities may be effected on each individual trajectory to further improve statistics.

This sampling scheme allows for a more efficient explo-

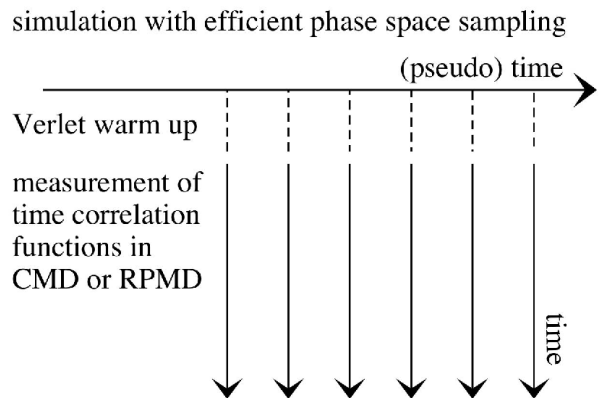


FIG. 2: Schematic representation of how to efficiently accumulate ergodic time correlation functions without distorting the dynamics during the observation stage.

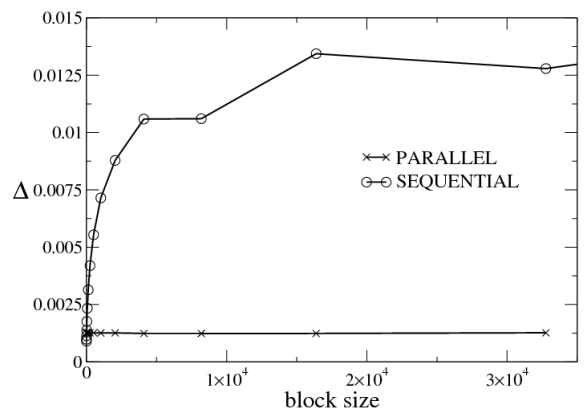


FIG. 3: Relative error in the mean  $\Delta$  (defined in Ref.<sup>57</sup>) of the virial estimator as a function of the block size for different sampling techniques in RPMD. Quartic potential  $V(x) = 0.25x^4$ ,  $\beta = 8$ , and  $P = 32$ . Circles: sequential sampling (previous works); Crosses: our suggested parallel sampling scheme.

ration of configuration space and is expected to improve statistics as the averages become less correlated than the sequential method. A quantitative measure of the error associated with each sampling technique is given in Fig. 3 for a particle in a purely quartic potential. The figure displays the relative error in the mean (see Eq.(2.3) of Ref.<sup>57</sup>) for the virial estimator<sup>58</sup> as a function of block size (number of steps between two consecutive velocity-rescale updates). The total number of observation steps in each sampling scheme remains constant, only differing in the way steps are distributed. It is evident that the sequential sampling has about an order of magnitude greater error than the parallel sampling, which converges at the beginning and stays constant thereafter. These magnitude of these errors agree with those of Ref.<sup>32</sup>.

The effect of the sampling method on the virial estimator was also investigated on a more realistic system. Fig. 4 displays the results for liquid *para*-hydrogen near

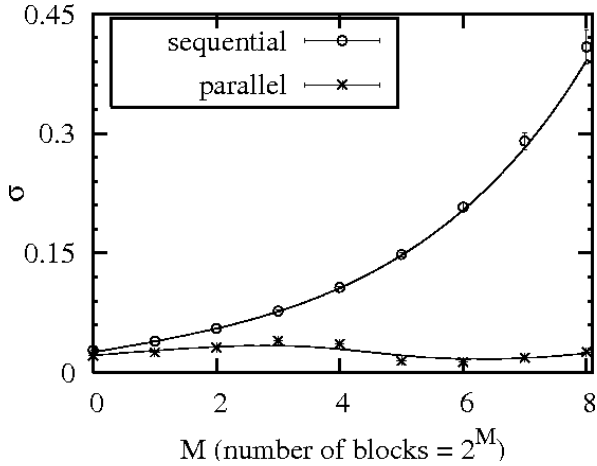


FIG. 4: Standard deviation of the virial estimator as a function of the number of blocks for different sampling techniques in RPMD. Liquid *para*-hydrogen at  $T = 14K$ , and  $P = 64$ . Circles: sequential sampling (previous works); Crosses: our suggested parallel sampling scheme.

its triple point,  $T = 14 K, \rho = 0.0235 \text{ \AA}^{-3}$ . The figure shows the more favorable convergence properties of the parallel sampling.

Finally, the rate of convergence of RPMD correlation functions versus number of trajectories was also investigated for each sampling method. Fig. 5 displays the mean absolute error  $\sigma = \frac{1}{N} \sum_{i=1}^N |K_{xx}(t_i) - K_{xx}^{conv}(t_i)|$  of each sampling method for various model systems.  $K_{xx}^{conv}$  denotes the fully converged RPMD correlation function for the system and  $K_{xx}$  is the resulting correlation function obtained from the cumulative average over consecutive trajectories (sequential sampling) or from statistically-independent trajectories (parallel sampling). The difference was computed up a maximum time of  $t_{max} = 10$  natural units (longer times comparisons are not meaningful) for the one dimensional systems. The total simulation time was equal for each sampling method for consistency. As a general trend, parallel sampling not only exhibits less statistical error associated but also converges faster than sequential sampling.

Similarly, Fig. 6 illustrates the impact of the sampling technique on the RPMD velocity autocorrelation function for liquid *para*-hydrogen at the same physical conditions given above. The difference was computed up a maximum time of  $t_{max} = 1$  picosecond. The sequential sampling curve is always above the parallel curve, indicating that the even for this more ergodic system the parallel sampling is useful.

Thus, the parallel sampling technique is recommended as a method for generating converged dynamical quantities, especially in cases where ergodicity problems are expected.

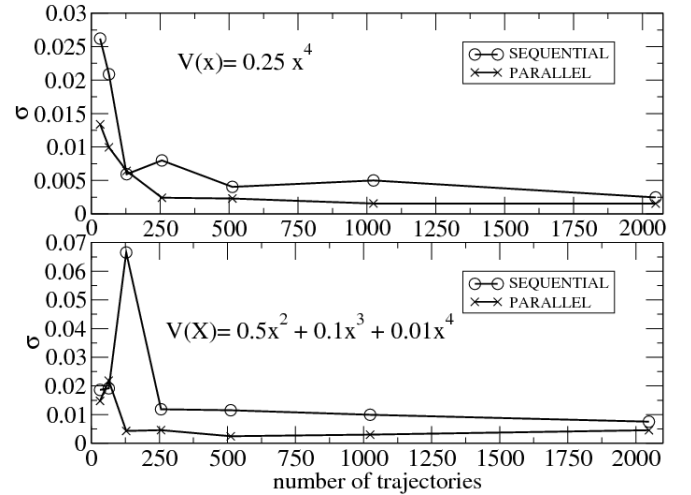


FIG. 5: Mean absolute error of the RPMD correlation functions  $\sigma = \frac{1}{N} \sum_{i=1}^N |K_{xx}(t_i) - K_{xx}^{conv}(t_i)|$  for parallel and sequential sampling methods.  $K_{xx}^{conv}$  is the fully converged Kubo-transformed position autocorrelation function. Above: quartic  $V(x) = 0.25x^4$  potential. Below: mildly anharmonic  $V(x) = 0.5x^2 + 0.1x^3 + 0.01x^4$  potential. A inverse temperature  $\beta = 8$  and Trotter number  $P = 32$  was used in both model potentials. The total number of steps was 60000 in each sampling method.

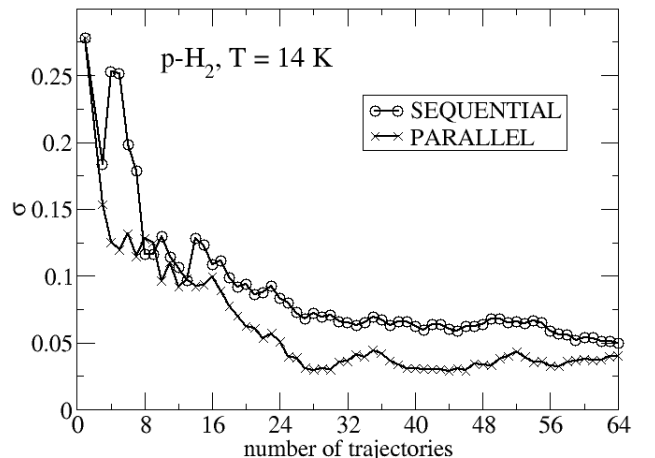


FIG. 6: Mean absolute error of the RPMD correlation functions  $\sigma = \frac{1}{N} \sum_{i=1}^N |K_{vv}(t_i) - K_{vv}^{conv}(t_i)|$  for parallel and sequential sampling methods.  $K_{vv}^{conv}$  is the fully converged Kubo-transformed velocity autocorrelation function for the *para*-hydrogen at  $T = 14K$  and  $P = 32$  obtained using RPMD. The number of steps per trajectory was 3500 and time step of 0.76 fs for each sampling method.

### G. Self-consistent quality control of time correlation functions

As argued in the introduction, it is desirable to have an internal consistency check for the predicted time correlation functions without relying on exact data (often not available in complex systems). From the simulations

(whether CMD or RPMD) and using Eq. (14) one obtains approximations to the standard velocity autocorrelation function  $\tilde{C}_{vv}(\omega)$ , which we denote by  $\tilde{C}_{vv}^{(\text{est})}(\omega)$ . Eq. (17) permits a reconstruction of the associated imaginary time correlation function  $G^{(\text{est})}(\tau)$  from  $\tilde{C}_{vv}^{(\text{est})}(\omega)$ . The estimated  $G^{(\text{est})}(\tau)$  function can then be compared directly to the numerically exact mean square displacement function  $G(\tau)$  computed from the same simulation, see Eq. (16). Thus, a dimensionless quantitative descriptor for the quality of an approach (CMD/RPMD) would be

$$\chi^2 = \frac{1}{\beta} \int_0^\beta d\tau \left[ \frac{G^{(\text{est})}(\tau) - G(\tau)}{G(\tau)} \right]^2. \quad (32)$$

An alternative way to carry out this comparative test would be to compare directly and on the same footing the imaginary-time velocity autocorrelation function  $G_{vv}(\tau)$ , Eq. 15 (see Ref.<sup>28</sup> and also Ref.<sup>30</sup> for a lowest-order estimator) to the one reconstructed from the real time velocity autocorrelation function using a similar expression as Eq. 17, but without the division by  $\omega^2$

$$G_{vv}(\tau) = \frac{1}{2\pi} \int_{-\infty}^{\infty} d\omega \exp(-\beta\omega/2) \times \tilde{C}_{vv}(\omega) \cosh \left[ \omega \left( \frac{\beta}{2} - \tau \right) \right]. \quad (33)$$

This approach, however, was not pursued here.

### III. COMPUTATIONAL DETAILS

In this section, we present the computational details for the model systems investigated. For the one-dimensional model systems, a total of 2048 independent trajectories of 130 natural units of time each were accumulated, according the scheme depicted in Fig. 2. Ten restarts on each individual trajectory are effected to further improve the statistics. The Trotter number was 8 and 32 for the high and low temperatures, respectively. For CMD, a converged adiabaticity parameter  $\gamma^2 = 0.005$  was used in all the low dimensional systems to scale down the non-centroid kinetic masses. The time step (after adiabatic separation) was 0.001. Nosé-Hoover chain thermostats<sup>37</sup> of length 2 were employed on the internal (non-centroid) modes to achieve proper canonical sampling. In the RPMD simulations the time step was 0.0005 to properly integrate all internal modes.

A realistic quantum fluid, *para*-hydrogen, was also simulated. The physical conditions of the system were chosen near its triple point ( $T = 14 \text{ K}, \rho = 0.0235 \text{ \AA}^{-3}$ ) to facilitate the comparison to preceding studies.<sup>22,50</sup> As usual, boson exchange effects are neglected at this temperature. The interaction between hydrogen molecules was modelled using the well-known isotropic Silvera-

Goldman (SG) potential.<sup>59</sup> This potential is given by

$$V(r) = e^{\alpha - \beta r - \gamma r^2} - \left( \frac{C_6}{r^6} + \frac{C_8}{r^8} - \frac{C_9}{r^9} + \frac{C_{10}}{r^{10}} \right) f_c(r), \quad (34)$$

where

$$f_c(r) = \begin{cases} \exp \left[ -\left( \frac{r_c}{r} - 1 \right)^2 \right], & \text{if } r \leq r_c \\ 1, & \text{otherwise.} \end{cases}$$

The parameters for the SG potential are displayed in Table (I). This potential has been shown to reproduce accurately static and dynamic properties in both solid and liquid phases.<sup>60</sup>

TABLE I: Parameters (in a.u.) in the Silvera-Goldman potential, Eq. (34).

$\alpha$	1.713	$C_6$	12.14
$\beta$	1.5671	$C_8$	215.2
$\gamma$	0.00993	$C_9$	143.1
$r_c$	8.321	$C_{10}$	4813.9

The system was composed of 256 particles initially arranged in an *fcc* lattice with periodic boundary conditions. The minimum image convention was adopted for the intermolecular interactions. The interaction between *para*-hydrogen molecules was truncated at 8.374 Å, corresponding to the second minimum in the radial distribution function. Initial velocities were drawn from a Maxwell-Boltzmann distribution at every restart to explore momenta space. A Trotter number of  $P = 32$  was sufficient to converge energy estimators at these physical conditions within a 97% margin of error. A full convergence of thermodynamic quantities is not sought here, but rather to compare the performance of each imaginary-time path integral method under the same simulation parameters.

Canonical sampling was achieved via Langevin thermostats. Although stochastic thermostats pose serious problems in the calculation of dynamical properties, they are very effective for rapid equilibration. In this study, the friction parameter  $\Gamma$  was carefully chosen so as not to disrupt the dynamical properties of the system. A friction coefficient of  $\Gamma = 0.01/dt$  typically makes systematic errors smaller than statistical errors.<sup>31</sup> No thermostats were directly applied to the centroids during CMD runs.

For CMD, the time scale separation between centroid and internal modes was set to 15 (adiabaticity parameter  $\gamma^2 = 0.0444$ ) and the time step to 0.2 fs. In order to facilitate exploration of configurational space, 64 independent trajectories were run for both methods with 2 restarts on each, following the scheme depicted in Fig. 2, giving a total of 128 trajectories. The duration of each trajectory was 6 ps. The time step used in RPMD was 0.76 fs to properly integrate all internal modes and ensure conservation of the total energy.

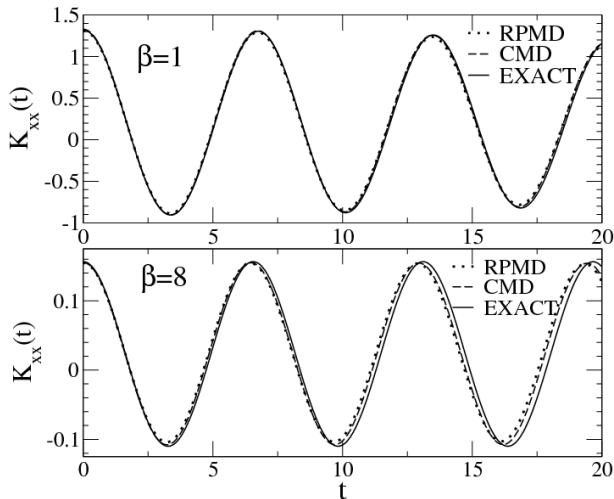


FIG. 7: Kubo-transformed position autocorrelation functions for the mildly anharmonic potential  $V(x) = 0.5x^2 + 0.1x^3 + 0.01x^4$  at two different temperatures.

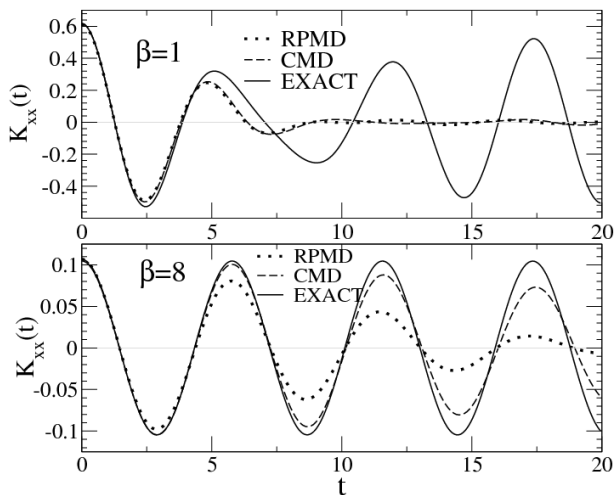


FIG. 8: Comparison of the Kubo-transformed position autocorrelation function for the purely quartic potential  $V(x) = 0.25x^4$  at two different temperatures.

## IV. RESULTS AND DISCUSSION

### A. One dimensional model potentials

Fig. 7 and Fig. 8 show the Kubo-transformed position autocorrelation functions for the mildly anharmonic and quartic potential, respectively. To facilitate comparisons to literature, the same inverse temperatures used in previous studies were employed here, namely,  $\beta = 1$  and 8, respectively.<sup>19,22</sup>

In general, the CMD and RPMD correlation functions agree well with each other and with exact results at times less than the thermal time. As expected, the agreement between CMD and the exact curves improves as the adiabatic separation between centroid and internal modes is

increased (not shown).

In the harmonic limit both methods are exact (at all times). Fig. 7 illustrates this point by showing the results on a slightly perturbed harmonic system. At high temperature ( $\beta = 1$ ) the agreement with exact curve is excellent in both methods. At lower temperature ( $\beta = 8$ ) however, the agreement is less satisfactory, with RPMD dephasing slightly more than the CMD at long times.

In anharmonic systems, CMD and RPMD suffer from a progressive loss of coherence and intensity as time goes on, which is especially significant for the quartic case at  $\beta = 1$ , Fig. 8, where both methods are dramatically quenched after the first oscillation.

At low temperatures, the quantum effects are more pronounced and both methods are expected to perform less favorably. Nonetheless, for the quartic case, the dynamics is curiously better described at low temperatures, whereas at high temperature the behavior is opposite. As pointed out by Voth *et al.*,<sup>15,22,61</sup> this behavior can be ascribed to the two-state nature of the system. At low temperature, the dynamics of the system is mostly dominated by the ground and first excited state. Therefore, it exhibits an effective harmonic behavior for which both approximate methods are exact. Interestingly, the quartic potential at  $\beta = 8$ , Fig. (8) shows that CMD can sustain oscillations longer than RPMD, which is severely quenched after few oscillations. The RPMD curve resembles the CMD signal but with the amplitude modulated by a decay function that results from the non-trivial effect of the damped dynamics internal modes on the centroid. This interesting effect can be easily explained by the following phenomenological argument. In RPMD the centroid dynamics contains admixture of higher frequencies modes (see later discussion on the power spectrum of a quantum fluid) which results in more damped behavior in the time correlation functions after averaging. Thus, each individual RPMD trajectory loses coherence more rapidly than CMD as time progresses.

Finally, a more challenging model potential for these approximate methods was investigated. Fig. 9 shows the Kubo-transformed position autocorrelation function of an asymmetric double well potential at  $\beta = 4$ . This potential crudely represents the typical scenario for a reduced coordinate in the vicinity of a quantum phase transition. As with any method that neglects quantum interference, neither RPMD nor CMD are able to describe the coherence in this deep tunneling case and the dynamics remains accurate only at very short times.

It should be pointed out that the dynamics in condensed phases is often dominated by the short-time behavior of correlation functions (provided that the density/pressure is not too high) and these methods are expected to become more meaningful as is illustrated in the next subsection.

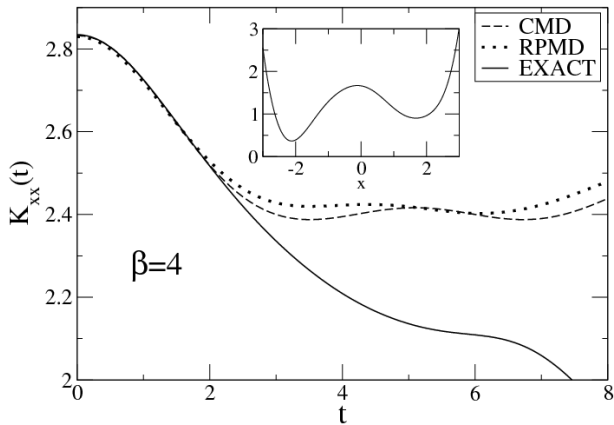


FIG. 9: Comparison of the Kubo-transformed position autocorrelation function for an asymmetric double well potential  $V(x) = 0.1(x^2 - 2)^2 + e^{-(x-2.2)^2} + 0.5e^{-(x+1.5)^2}$  at  $\beta = 4$  and  $P = 32$ : Exact (solid), RPMD (dots), and adiabatic CMD (dashes). The bare potential is shown in the inset.

### B. Liquid *para*-hydrogen

In this section the comparative study of a realistic quantum fluid system is presented.

Fig. 10 displays the Kubo-transformed velocity autocorrelation function for *para*-hydrogen. Both correlation functions look very similar, and feature a prominent negative minimum at about 0.24 ps, a little bump around 0.4 ps, followed by a fast decay after 1 ps. The RPMD curve is, however, noticeably displaced to the left relative to the CMD curve. This observation is consistent with the general trend of RPMD correlation functions to relax faster than CMD (see following discussion on diffusion constants). Table (II) displays the values of the velocity autocorrelation function at few selected points for each method.

TABLE II: The Kubo-transformed velocity autocorrelation function [ $\text{\AA}^2/\text{ps}$ ] at various selected points for *para*-hydrogen at  $T = 14$  K,  $\rho = 0.0235$   $\text{\AA}^{-3}$  with  $N = 256$ . The standard deviation in the last digit is given in parentheses.

Time[ps]	CMD	RPMD
0.0	17.42(4)	17.45(2)
0.156	0.92(3)	0.41(1)
0.238	-2.96(1)	-3.08(1)
0.50	-0.60(1)	-0.657(3)
0.751	-0.13(1)	-0.14(1)

Table (III) lists the values of the self-diffusion coefficient for *para*-hydrogen computed from the well-known Green-Kubo relation<sup>45</sup>

$$D = \frac{1}{3} \int_0^\infty K_{vv}(t) dt. \quad (35)$$

Values in Table (III) are in accord with previously re-

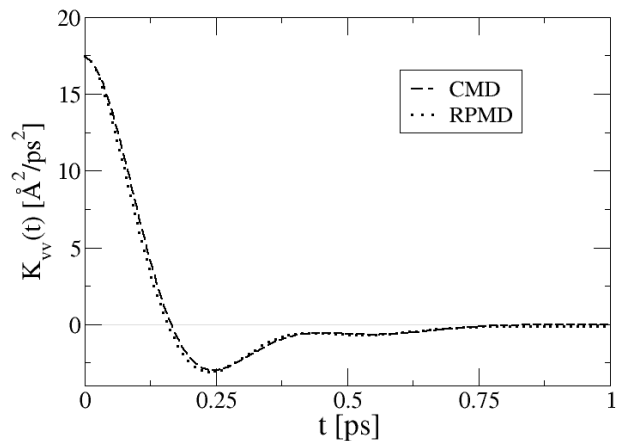


FIG. 10: Kubo-transformed velocity autocorrelation function for *para*-hydrogen at  $T = 14$  K,  $\rho = 0.0235$   $\text{\AA}^{-3}$  as computed from adiabatic CMD (dashes) and RPMD (dots).

ported data.<sup>22,50</sup> In particular, the predicted RPMD value (0.262  $\text{\AA}^2/\text{ps}$ ) is in excellent agreement with a recent study by Miller and Manolopoulos.<sup>50</sup> Our CMD value for the self-diffusion constant agrees very well with the one reported in Ref.<sup>22</sup> and the small discrepancy (0.01) is attributed to different simulation parameters. As a consistency check, the diffusion constants were also estimated from the long-time behavior of the mean square displacement (not shown) and found perfect agreement with those from Eq. (35). Finally, we note that these computed diffusion coefficients should be extrapolated to the infinite case for better agreement with the experiment.<sup>50</sup> Conversely, the experimental value could also be “corrected” for finite size effects<sup>62</sup> and then compared directly to the values from the simulations.

TABLE III: Self-diffusion coefficient for *para*-hydrogen at  $T = 14$  K,  $\rho = 0.0235$   $\text{\AA}^{-3}$  with  $N = 256$  as computed from path integral methods. The experimental value is from Ref.<sup>63</sup>. The standard deviation in the last digit is given in parentheses.

Diffusion coefficient $D[\text{\AA}^2/\text{ps}]$	
Experiment	0.4
CMD	0.310(4)
RPMD	0.262(1)

Fig. (11) shows the imaginary-time correlation function, Eq. (16), and its reconstructed version (computed from Eq. (17)) for each path integral method. The imaginary-time mean square displacement (ITMSD) function (“ima”, in the figure) is virtually identical in both RPMD and CMD, indicating a converged sampling. The reconstructed RPMD ITMSD (dots) appears to be slightly farther than CMD (dashes) from its respective imaginary-time correlation function. Eq. (17) was used to quantitatively assess this difference, and the numerical values are also presented in Fig. 11. RPMD exhibits a

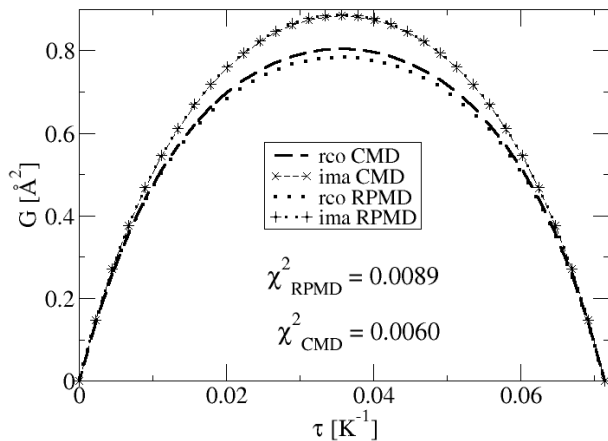


FIG. 11: Comparison of the imaginary-time mean square displacement correlation function (“ima”, in the figure) as given by Eq. (16), and its reconstructed version (“rco” in the figure) from Eq. (17) for *para*-hydrogen at  $T = 14$  K,  $\rho = 0.0235$  Å<sup>-3</sup>. The  $\chi^2$  error as defined in Eq. (17) is shown for each method.

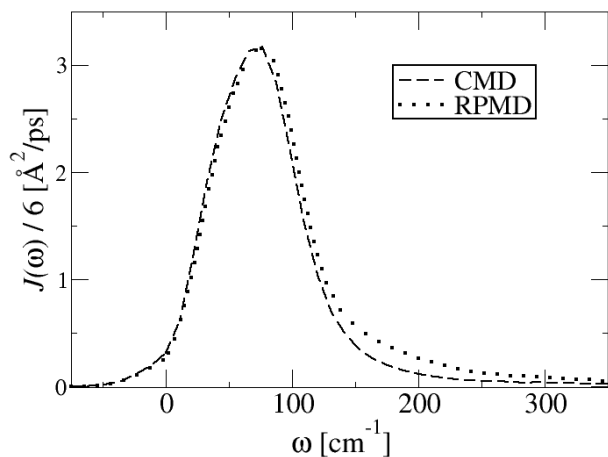


FIG. 12: Comparison of the computed Fourier transform of the standard velocity autocorrelation function for *para*-hydrogen at  $T = 14$  K,  $\rho = 0.0235$  Å<sup>-3</sup>. Only the real part is shown.

slightly poorer convergence than CMD under the same simulation parameters (total observed time, etc). Thus, the  $\chi^2$ -test indicates that both methods perform very similarly in recovering dynamical information.

As a further investigation of the differences between both methods, the power spectrum of the standard velocity autocorrelation function<sup>22</sup>

$$J(\omega) = \int_{-\infty}^{\infty} C_{vv}(t) e^{i\omega t} dt, \quad (36)$$

was computed for *para*-hydrogen and its real part is

shown in Fig. (12). In both methods, the spectrum looks very similar at low and mid frequencies and features a strong asymmetric peak at  $75$  cm<sup>-1</sup>. The only difference arises at higher frequencies. This fact provides some insight into the physical difference between the path integral methods. The RPMD spectrum reveals a significant presence of high frequency centroid vibrations (due to undamped internal modes) as already pointed out by Voth *et al.*<sup>22</sup>. This has a direct effect on the centroid dynamics causing a faster relaxation in the correlation functions and thereby leading to a smaller value for the self-diffusion constants (Table (III)). In contrast, in CMD, the effect of the thermostats on the internal modes results in a smoother centroid dynamics and hence, less damping in the correlation functions. This results in a slightly better reconstructed imaginary time correlation functions and hence a somewhat smaller  $\chi^2$  error.

## V. CONCLUSIONS

In this paper, we have addressed the problem of ergodic sampling in the centroid and ring-polymer molecular dynamics techniques, and we have introduced an internal consistency descriptor  $\chi^2$  for assessing the accuracy of the approximate quantum time correlation functions. In addition, we have discussed the physical differences between imaginary time path integral methods, CMD and RPMD. These methods were compared numerically for a variety of model systems using an improved sampling technique to remedy any potential non-ergodic behavior. The computed values from linear correlation functions are very similar in condensed phases (*para*-hydrogen), and both method yield similar performance in recovering imaginary time correlation functions. However, in less ergodic systems such as the purely quartic system at low temperature the approximate methods differ significantly. In this model system, the resulting RPMD correlation function evidences a more damped behavior due to effect of internal modes on the centroid motion. In contrast, this effect is less severe in CMD owing to the averaging effect of the thermostats on the high-frequency modes of the ring polymer.

## Acknowledgments

The authors would like to thank Serge Ivanov for critical reading on an early draft of this manuscript, Dominik Marx for some comments, Debashish Mukherji for some help with the RPMD code, and the anonymous reviewers for their valuable comments.

- \* mark.tuckerman@nyu.edu; <http://homepages.nyu.edu/~mt33/>; MET acknowledges support from NSF CHE-0704036 and from PRF45485-AC5
- † mmuser@uwo.ca; <http://publish.uwo.ca/~mmuser/>; MHM acknowledges financial support from NSERC and PREA.
- <sup>1</sup> R.P. Feynman (editor: L.M. Brown.). *A new approach to Quantum Theory (Feynman's thesis)*. World Scientific, Singapore, (2005).
  - <sup>2</sup> R. P. Feynman, Rev. Mod. Phys. **20**, 367–387 (1948).
  - <sup>3</sup> D. M. Ceperley, Rev. Mod. Phys. **67**, 279–355 (1995).
  - <sup>4</sup> J. Liu and W. H. Miller, J. Chem. Phys. **127**, 114506 (2007).
  - <sup>5</sup> J. Liu and W. H. Miller, J. Chem. Phys. **128**, 144511 (2008).
  - <sup>6</sup> D. R. Reichman and E. Rabani, Phys. Rev. Lett. **87**, 265702 (2001).
  - <sup>7</sup> E. Rabani and D. R. Reichman, Annu. Rev. Phys. Chem. **56**, 157–185 (2005).
  - <sup>8</sup> E. Rabani and D. R. Reichman, Phys. Rev. E **65**, 036111 (2002).
  - <sup>9</sup> D. R. Reichman and E. Rabani, J. Chem. Phys. **116**, 6279 (2002).
  - <sup>10</sup> E. Rabani and D. R. Reichman, J. Chem. Phys. **120**, 1458–1465 (2004).
  - <sup>11</sup> A. Nakayama and N. Marki, J. Chem. Phys. **119**, 8592 (2003).
  - <sup>12</sup> A. Nakayama and N. Marki, J. Chem. Phys. **125**, 024503 (2006).
  - <sup>13</sup> J. A. Poulsen, G. Nyman and P. J. Rossky, Proc. Natl Acad. Sci. USA **102**, 6709–6714 (2005).
  - <sup>14</sup> A. Horikoshi and K. Kinigawa, J. Chem. Phys. **119**, 4629 (2003).
  - <sup>15</sup> J. Cao and G.A. Voth, J. Chem. Phys. **99**(12), 10070–10073 (1993).
  - <sup>16</sup> J. Cao and G.A. Voth, J. Chem. Phys. **100**(7), 5106–5117 (1994).
  - <sup>17</sup> H. Kim and P.J. Rossky, J. Phys. Chem. B **106**(33), 8240–8247 (2002).
  - <sup>18</sup> H. Kim and P.J. Rossky, J. Chem. Phys. **125**(7), 074107 (2006).
  - <sup>19</sup> I.R. Craig and D.E. Manolopoulos, J. Chem. Phys. **121**(8), 3368–3373 (2004).
  - <sup>20</sup> M. Parrinello and A. Rahman, J. Chem. Phys. **80**(2), 860–867 (1984).
  - <sup>21</sup> B.J. Braams and D.E. Manolopoulos, J. Chem. Phys. **125**(12), 124105 (2006).
  - <sup>22</sup> T.D. Hone, P.J. Rossky and G.A. Voth, J. Chem. Phys. **124**(15), 154103 (2006).
  - <sup>23</sup> R. M. Lynden-Bell and K. H. Michel, Rev. Mod. Phys. **66**(3), 721–762 (1994).
  - <sup>24</sup> M. Holz, X. Mao, D. Seiferling and A. Sacco, J. Chem. Phys. **104**(2), 669–679 (1996).
  - <sup>25</sup> G. Baym and D. N. Mermin, J. Math. Phys. **2**(2), 232–234 (1961).
  - <sup>26</sup> Berne B. J. and D. Thirumalai, Annu. Rev. Phys. Chem. **37**(1), 401–424 (1986).
  - <sup>27</sup> E. Rabani, G. Krilov and B. J. Berne, J. Chem. Phys. **112**, 2605 (2000).
  - <sup>28</sup> E. Rabani, D. R. Reichman, G. Krilov and B. J. Berne, Proc. Natl Acad. Sci. USA **99**, 1129–1133 (2002).
  - <sup>29</sup> E. Rabani, G. Krilov, D. R. Reichman and B. J. Berne, J. Chem. Phys. **123**, 184506 (2005).
  - <sup>30</sup> B. J. Braams and D. E. Manolopoulos, J. Chem. Phys. **127**, 174108 (2007).
  - <sup>31</sup> F.R. Krajewski and M.H. Müser, J. Chem. Phys. **122**(12), 124711 (2005).
  - <sup>32</sup> M.E. Tuckerman, B.J. Berne, G.J. Martyna and M.L. Klein, J. Chem. Phys. **99**(4), 2796–2808 (1993).
  - <sup>33</sup> R.P. Feynman and A.R. Hibbs. *Quantum Mechanics and Path Integrals*. McGraw-Hill, New York, (1965).
  - <sup>34</sup> D. Chandler and P. G. Wolynes, J. Chem. Phys. **74**, 4078 (1981).
  - <sup>35</sup> R. W. Hall and B. J. Berne, J. Chem. Phys. **81**, 2523 (1984).
  - <sup>36</sup> E. L. Pollock and D. M. Ceperley, Phys. Rev. B **30**, 2555 (1984).
  - <sup>37</sup> G.J. Martyna, M.L. Klein and M.E. Tuckerman, J. Chem. Phys. **97**(4), 2635–2643 (1992).
  - <sup>38</sup> J. S. Cao and G. A. Voth, J. Chem. Phys. **101**, 6168 (1994).
  - <sup>39</sup> M. E. Tuckerman, D. Marx, M. L. Klein and M. Parrinello, J. Chem. Phys. **104**, 5579 (1996).
  - <sup>40</sup> D. Marx, Tuckerman M.E. and Martyna G.J., Comput. Phys. Comm. **118**(2), 166–184 (1999).
  - <sup>41</sup> G.J. Martyna, A. Hughes and M.E. Tuckerman, J. Chem. Phys. **110**(7), 3275–3290 (1999).
  - <sup>42</sup> M. H. Müser, Comput. Phys. Comm. **147**(2), 83–86 (2002).
  - <sup>43</sup> L. D. Landau and E. M. Lifshitz. *Statistical Physics*. Pergamon Press, New York, (1968).
  - <sup>44</sup> D. Thirumalai, E.J. Bruskin and B.J. Berne, J. Chem. Phys. **79**(10), 5063–5069 (1983).
  - <sup>45</sup> R. Kubo, M. Toda, and N. Hashitsume. *Statistical Physics II: Nonequilibrium Statistical Mechanics*. Springer, New York, (1985).
  - <sup>46</sup> R. P. Feynman and H. Kleinert, Phys. Rev. A **34**, 5080 (1986).
  - <sup>47</sup> M. J. Gillan, J. Phys. C. **20**(24), 3621 (1987).
  - <sup>48</sup> J. Cao and G.A. Voth, J. Chem. Phys. **104**(1), 273–285 (1996).
  - <sup>49</sup> J. Cao and G. J. Martyna, J. Chem. Phys. **104**(5), 2028–2035 (1996).
  - <sup>50</sup> T.F. Miller III and D.E. Manolopoulos, J. Chem. Phys. **122**(18), 184503 (2005).
  - <sup>51</sup> T. F. Miller III and D.E. Manolopoulos, J. Chem. Phys. **123**(15), 154504 (2005).
  - <sup>52</sup> I.R. Craig and D.E. Manolopoulos, Chemical Physics **322**(1-2), 236–246 (2006).
  - <sup>53</sup> I.R. Craig and D.E. Manolopoulos, J. Chem. Phys. **122**(8), 084106 (2005).
  - <sup>54</sup> M. E. Tuckerman, B. J. Berne and G. J. Martyna, J. Chem. Phys. **97**(10), 1990 (1992).
  - <sup>55</sup> S. Thomas, D. Burkhard and K. Kurt, Phys. Rev. E **68**(4), 046702 (2003).
  - <sup>56</sup> I. Vattulainen P. Nikunen M. Karttunen, Comput. Phys. Comm. **153**(3), 407–423 (2003).
  - <sup>57</sup> J. Cao and B.J. Berne, J. Chem. Phys. **91**(10), 6359–6366 (1989).
  - <sup>58</sup> M. F. Herman, E. J. Bruskin and B. J. Berne, J. Chem. Phys. **76**(10), 5150 (1982).
  - <sup>59</sup> I.F. Silvera and V.V. Goldman, J. Chem. Phys. **69**(9), 4209–4213 (1978).

- <sup>60</sup> D. Scharf, G.J. Martyna and M.L. Klein, *Low Temp. Phys.* **19(5)**, 364–367 (1993).
- <sup>61</sup> S. Jang and G.A. Voth, *J. Chem. Phys.* **111(6)**, 2371–2384 (1999).
- <sup>62</sup> I. C. Yeh and G. Hummer, *J. Phys. Chem. B* **108(40)**, 15873 (2004).
- <sup>63</sup> edited by B. N. Eselson, Y. P. Blagoi, V. V. Geigoriev, V. G. Manzheli, S. A. Mikhailenko and N. P. Neklyndov. *Properties of Liquid and Solid Hydrogen*. Israel Program for Scientific Translation, Jerusalem, (1971).